Excitation and quenching mechanisms in the near-UV photodissociation of CH₃Br and CH₃Cl adsorbed on D₂O or CH₃OH on Cu(110)

E. T. Jensen

Photochemical processes for CH₃X (X = Cl, Br, I) adsorbed on top of thin films of D₂O or CH₃OH on a Cu(110) substrate is studied by time-of-flight mass spectrometry for a range of UV wavelengths (351–193 nm). Photodissociation *via* dissociative electron attachment by photoelectrons and by neutral photodissociation is identified and quantified based on the observed dynamics of the desorbing CH₃ fragments. Photoelectron-driven dissociation of CH₃X is found to be a maximum for monolayer quantities of the D₂O or CH₃OH on Cu(110), but with differing kinetic energy release on the two substrates. The dynamics of CH₃Br and CH₃Cl photodissociation qualitatively differ on CH₃OH/Cu(110) as compared to D₂O/Cu(110), which is ascribed to differing molecular structures for these systems. Evidence is presented for an efficient inter-molecular quenching mechanism for neutral photoexcitation of CH₃Cl and CH₃Br on the CH₃OH/Cu(110) substrate.

1 Introduction

There has been much recent work reported on UV photon- and electron-driven chemical processes in heterogeneous molecular thin films, particularly for water ices. These studies are driven by interests in astrochemistry and planetary science,[1–3] as well as terrestrial processes as seen in radiation chemistry[4,5] and photocatalysis.[6,7] A wide range of surface science techniques have been applied to studying these systems. To date there have been relatively few studies of photodissociation dynamics in these types of heterogeneous systems. We have studied a range of halomethanes (CH₃X, X = Cl, Br, I) adsorbed on thin films of D₂O or CH₃OH on Cu(110) substrate. The stimulated dissociation properties of these halomethanes have been studied in some detail in both the gas-phase as well as condensed on surfaces. Depending on the context, these molecules can display low-energy photoelectron driven Dissociative Electron Attachment (DEA) or neutral photodissociation processes when in the adsorbed state.

The solid ices of D₂O and CH₃OH have large bandgaps, with the onset of absorption in solid methanol near 6.7 eV ($\lambda < 184$ nm),[8] while for water the absorption onset is 8.5 eV.[9] However these molecules are known to play roles in electron-driven chemistry in a variety of systems, as the dipolar molecules can solvate low-energy electrons such as photoelectrons[10] or impinging external electrons.[11] The solvation dynamics of electrons at thin water films on metal substrates has been

studied extensively by two-photon photoemission.[10,12] Several studies have implicated electron transfer at water–halocarbon interfaces as being responsible for halocarbon dissociation.[11,13,14] Photoelectron dynamics and solvation on CH₃OH[15–17] thin films been studied using two-photon photoemission by a variety of research groups, and is known as a 'hole-getter' when adsorbed on TiO₂.[18]

The surface chemistry and photochemistry of methyl halides on a variety of metal surfaces has been the subject of many studies,[19] as has the adsorption of water[20,21] and methanol.[22,23] There are several previous studies that have looked at the coadsorption systems of methyl halides with water, most particularly chloromethane and water. Due primarily to the electrostatic dipole moments of these species, the interactions between CH₃Cl and D₂O on metals are characterized by repulsion, and has been investigated by temperature programmed desorption (TPD) and modelling studies by Maschhoff *et al.*[24] who concluded that the long range electrostatic dipole–dipole interactions are an important factor in the CH₃Cl structures. The CH₃Cl binding energies were found to decrease with increasing coverage of D₂O and CH₃Cl, and the repulsive interactions cause CH₃Cl islands to form atop the preadsorbed D₂O or between D₂O islands. Similar conclusions are reached by Lilach and Asscher,[25] studying CH₃Cl and H₂O on Ru(100), and inferred the net orientation of the CH₃Cl dipoles from work-function changes during adsorption and TPD. A recent study of CH₃Cl and D₂O on Pd(111) by Fournier *et al.* using sum-frequency generation (SFG) spectroscopy[26] concluded that the CH₃Cl adsorbs onto the D₂O through hydrogen bonding between the D and Cl atoms and that the O–D–Cl–CH₃ bonds

Department of Physics, University of Northern BC, 3333 University, Way, Prince George B.C., V2N 4Z9, Canada. E-mail: ejensen@unbc.ca; Tel: +1-250-960-6463

This journal is © the Owner Societies 2015

Phys. Chem. Chem. Phys., 2015, **17**, 9173–9185 | 9173

are aligned close to the surface normal, though with wider angular variation than for Cl–CH$_3$ on the bare metal surface. Their SFG results also indicate that the large Cl electronegativity induces a partial charge transfer between the surface and the D$_2$O. There have been several previous studies of photochemistry in these systems – using a UV Hg arc lamp ($h\nu > 5.4$ eV) to irradiate CH$_3$Cl/D$_2$O/Pt(111), Jo and White[27] highlighted the role of low energy photoelectrons in the observed CH$_3$Cl photodissociation, and the rapid diminution of the transport of the relevant photoelectrons as the D$_2$O layer thickness was increased.

There are relatively few previous studies of the dynamics of photodissociation in these heterogeneous systems, in which the mechanisms of photodissociation can be analyzed from the photofragment translational energies. We recently published a study of CH$_3$I/D$_2$O/Cu(110) photodissociation at $\lambda = 248$ nm in which the CH$_3$ photofragment translational energies were analyzed to highlight the varying contributions from neutral photodissociation and photoelectron dissociative electron attachment mechanisms.[28] A study of CH$_3$I on thick D$_2$O layers[29] analyzed the ground- and excited state I atoms emitted subsequent to $\lambda = 260$ nm and 290 nm photodissociation. These studies showed evidence for a proportion of the I-atoms having larger than gas-phase translational energies which was ascribed to "chattering" during dissociation from 'methyl-down' oriented molecules on the ice surface as well as fast CH$_3$ photofragments leaving the surface from 'methyl-up' oriented molecules.

1.1 Energetics of stimulated dissociation

If one begins by considering the dissociation of a CH$_3$X molecule in free space, then the requirements of momentum and energy conservation put a limit on how the excess kinetic energy is partitioned between the CH$_3$ fragment and the halogen atom. For a DEA process the following can be used to rationalize the CH$_3$ photofragment kinetic energy in terms of the component energy factors:

$$T_{CH_3} = \frac{m(X)}{m(CH_3X)}\{E_{e^-} + EA(X) - D_0(C-X) + \Delta E_{solv}(X^-) - E_{int}(CH_3)\} \tag{1}$$

where $m()$ is the mass of the particular species, E_{e^-} is the incident electron energy, $EA(X)$ is the electron affinity for the halogen atom X, D_0 is the energy of the bond being broken, $\Delta E_{solv}(X^-)$ is the energy of solvation for the product anion in its dielectric environment and $E_{int}(CH_3)$ is the internal energy (vibration and rotation) of the departing methyl fragment. In principle the solvation energy can be estimated (e.g. ref. 30 and 31) but the uncertainty in various parameters leads to ΔE_{solv} values that have large uncertainty. This is particularly true in the heterogeneous molecular environments of dipolar molecules that we are considering in the present work, in which the solvation energy is structure and site sensitive, and can shift dynamically as the dissociation proceeds. The photoelectron energy E_{e^-} in surface photodissociation is normally taken to be selected from the range of photoelectron energies created by the incident photons at the

metal–molecule–vacuum interface,[32] and so from the range of photoelectron energies between the Fermi energy E_F and $E_F + h\nu$.

For neutral photodissociation, the analogous equation is:

$$T_{CH_3} = \frac{m(X)}{m(CH_3X)}\{h\nu - D_0(C-X) - E_{int}(X) - E_{int}(CH_3)\} \tag{2}$$

where $h\nu$ is the photon energy, and $E_{int}(X)$ allows for the possible electronic excitation of the departing halogen atom. In surface systems the parent molecule is not in free space, but embedded at or near the vacuum interface of the system being studied. It is known from prior work in surface photochemistry that the observed fragment kinetic energy distributions can be altered by chemical or post-dissociation interactions, however eqn (1) and (2) provide a basis to begin consideration of the observed kinetic energy distributions.

Gas-phase photodissociation of CH$_3$Br[33,34] and CH$_3$Cl[35] at $\lambda = 193$ nm occurs in the 'A-band', a set of overlapping excited electronic states. In contrast to the better known case of CH$_3$I A-band photodissociation, the 193 nm photodissociation of CH$_3$Br and CH$_3$Cl is dominated by a perpendicular transition from the ground state, mainly via the $^1Q_1$ state, which correlates to dissociation to CH$_3$ and a ground-state halogen atom. For CH$_3$Br there is evidence[34] for non-adiabatic coupling with the $^3Q_0$ state, which leads to CH$_3$ and electronically excited Br*. Given the experimental geometry used in our work, these neutral photodissociation channels are accessible in the experiments we describe below.

For either A-band neutral photodissociation or photoelectron driven DEA of the halomethanes, the dissociation process is direct, with bond-breaking occurring in a few tens of femtoseconds. Photodissociation of halomethanes adsorbed on or close to a metal surface can be inhibited by quenching.[36,37] When several layers of halomethanes are adsorbed, or are adsorbed on top of a spacer layer of another species, both DEA and neutral photodissociation have been observed. Quenching of one or both photodissociation pathways by the metal surface at these timescales requires a rapid interaction, such as resonant electron–hole transfer between the excited molecule and the substrate.[37]

2 Experimental details

The experiments were performed in an ultra-high vacuum system that has been described previously.[38] The Cu(110) single crystal sample is cooled by liquid nitrogen (base temperature 90 K) and can be heated by electron bombardment to 920 K for cleaning. Sample cleanliness and order were monitored by Auger electron spectroscopy and low energy electron diffraction measurements respectively.

Neutral products from surface photodissociation travel 185 mm to pass through a 4 mm diameter aperture to a differentially pumped Extrel quadrupole mass spectrometer (QMS) with an axial electron bombardment ionizer. The sample to ionizer distance is 203 mm. Ions created in the ionizer then

9174 | Phys. Chem. Chem. Phys., 2015, 17, 9173–9185

This journal is © the Owner Societies 2015

travel through the quadrupole region and are mass selected, in the present experiments using m/z = 15 amu. Ion arrivals are recorded using a multichannel scaler that begins counting 50 μs prior to the initiating laser pulse, and the counts recorded from multiple laser pulses are summed. Unless otherwise indicated, the spectra shown in the present work are the result of summing data from 1000 laser pulses into 1000 1 μs time bins. In order for the ion arrival times to reflect the neutral fragment time-of-flight, they are corrected for the ion flight time (for CH_3^+, 17 μs at the 50 eV ion energy used in the QMS). This is the leading systematic uncertainty in the recorded flight times (± 1.5 μs) which does not affect comparisons between different TOF spectra but does lead to fixed nonlinear systematic uncertainty in the reported fragment kinetic energies (KE $\propto 1/(TOF)^2$), which is most problematic at short flight times. The TOF spectra $N(t)$ were converted to probability distributions versus CH_3 kinetic energy ($P(E)$) using the Jacobian transformation with a correction factor $1/t$ to account for the reduced ionization probability of faster neutral CH_3 fragments.

The laser pulses (~ 5 ns duration) are produced by a small excimer laser (MPB PSX-100) operating at 20 Hz. In this work 351 nm (XeF), 308 nm (XeCl), 248 nm (KrF) and 193 nm (ArF) laser light was used, with laser fluences on the sample of ~ 0.8 mJ cm^{-2} or less per pulse, depending on the wavelength used. Linearly polarized light has been used exclusively in this work. To create polarized light, the beam passes through a birefringent MgF$_2$ crystal to separate p- and s-polarized components, which can then be directed at the sample. All of the TOF spectra shown in the present work were obtained using p-polarized light, though we also acquired data using s-polarized light for comparison.† The laser pulses were collimated using a 6 mm diameter aperture and were unfocussed on the sample. The laser light is incident upon the sample at a fixed angle of 45° from the mass spectrometer axis – for example, when the Cu(110) sample is oriented to collect desorption fragments along the surface normal direction, the light is incident at 45°.

Deposition of molecules on the sample is done using a microcapillary array directed doser,[39] with the sample held normal to the doser, 25 mm away. This was found to enhance the deposition by a factor of 10 compared to background dosing. The CH$_3$Br (Aldrich, $\geq 99.5\%$) and CH$_3$Cl (Aldrich, $\geq 99.5\%$) gas used in this work was transferred via a glass and teflon gas-handling system. The CH$_3$I (Aldrich, 99.5%) dosing used room temperature vapour from the liquid. The D$_2$O (Aldrich, 99.9 atom% D) and CH$_3$OH (Aldrich, $\geq 99.9\%$) used in this work was degassed by multiple freeze–pump–thaw cycles and was contained in a pyrex vial a few cm from the precision leak valve used to admit gases to the directed doser. The CH$_3$Br dosing was calibrated by temperature programmed desorption measurements. In this case, 0.95 ± 0.05 L CH$_3$Br was found to correspond to 1.0 ML for that substrate. In the

present case of adsorption of CH$_3$Br on D$_2$O thin films in which the surface structure is less well characterized and no distinct TPD or photochemical signatures define what dose corresponds to monolayer CH$_3$Br, we report CH$_3$Br doses in terms of effective monolayers based on this calibration (1.0 ML = 0.95 L). For D$_2$O we determined an effective monolayer calibration based on findings from TPD and titration of CCl$_4$ on top of varying D$_2$O films, which formed atomic chlorine on the metal surface after warming to desorb the molecular layers. From this we found 1.0 ML = 0.30 L for D$_2$O. A similar procedure was used to calibrate the dosing of CH$_3$OH, where 0.35 L was equivalent to 1 ML coverage. In deposition of these molecules, we assumed unit sticking probability on the various substrates for the temperature used for dosing ($T < 95$ K).

Details of the adsorption structures found for D$_2$O/Cu(110) has been the subject of a number of studies, and is summarized in ref. 21. Less detail is available on the structure of CH$_3$OH/Cu(110), though a study using IR spectroscopy[40] indicates that the first layer adsorbs uniformly, and that 3D crystallites grow in the multilayer regime. It is also possible that the D$_2$O or CH$_3$OH structures are perturbed by the coadsorption of the dipolar CH$_3$X molecules.[24] In the results reported in the present work, we have looked for changes in photochemical behaviour as the different molecular coverages were varied, in part as a means to understand what structural changes might be occurring.

3 Results and discussion

3.1 Photodissociation at 248 nm on D$_2$O/Cu(110)

Time-of-flight spectra at 15 amu for CH$_3$Br adsorbed on D$_2$O/Cu(110) obtained using 248 nm ($h\nu$ = 5.0 eV) light show two main features, as illustrated in Fig. 1 – a photodissociation feature that peaks near 60 μs flight time and a broad, slow photodesorption feature centered around 500 μs flight time.
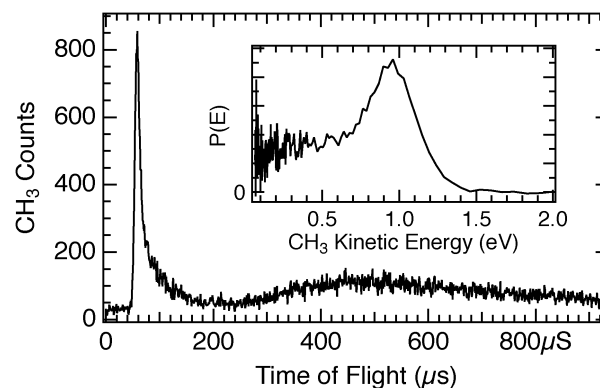

Fig. 1 Time of flight spectrum from the photodissociation of 0.7 ML of CH$_3$Br adsorbed on 1.0 ML D$_2$O/Cu(110) detected at 15 amu (CH$_3^+$) following 248 nm irradiation. The peak at 58 μs flight time is due to photodissociation of the CH$_3$Br and the slower broad peak (500 μs) is a result of photodesorption of CH$_3$Br molecules that dissociate in the mass spectrometer ionizer. The inset plot shows the same data transformed to a probability distribution as a function of CH$_3$ kinetic energy.

† For work at 248 nm and 308 nm, s-polarized light was derived from the p-polarized beam by inserting an antireflection coated zero order half-waveplate into the beam. For 193 nm and 351 nm, s-polarized light was obtained by rotating the MgF$_2$ crystal to direct the s-polarized beam onto the sample.
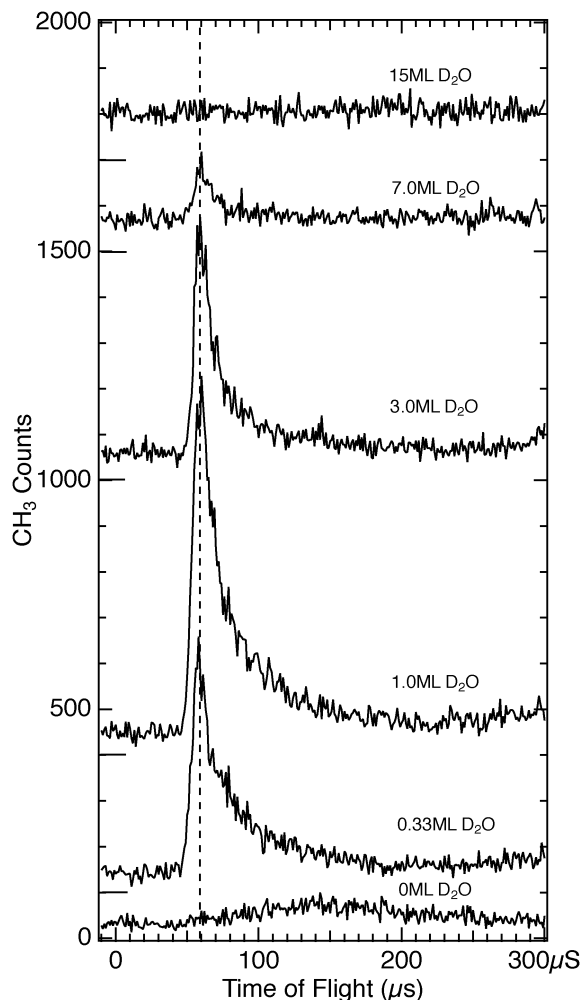
Fig. 2 Sequence of time of flight spectra from 1 ML of CH_3Br on D_2O/Cu(110) obtained using a varying amount of D_2O and 248 nm light. The CH_3Br photodissociation feature at 58 μs flight time increases rapidly as the first monolayer of D_2O is added, and then diminishes as the D_2O layer thickness is increased.

Fig. 3 The yield of CH_3 photofragments obtained from 248 nm photo-dissociation (red circles) and photodesorption (blue triangles) of 1 ML CH_3Br on D_2O/Cu(110) as a function of D_2O dose. The solid line represents a simple exponential decay fit to the data points from 1.0 ML D_2O and higher—essentially the same fitted function is obtained from either the photodissociation or the photodesorption data.

Although the data of Fig. 3 display a smoothly changing photo-chemical yield as the D_2O coverage is increased, this does not necessarily mean that the D_2O layer growth is uniform. However the diminution of the photoelectron-driven signal does show that the average distance from the substrate to the CH_3Br target that is detected in TOF increases with the D_2O coverage.

The photodissociation of CH_3Cl on D_2O/Cu(110) at 248 nm has also been studied, with a representative TOF spectrum shown in Fig. 4. The yield of CH_3 photofragments from CH_3Cl on D_2O/Cu(110) is much lower than that seen for CH_3Br, and the spectrum shown is an average of 3 spectra, in order to improve the signal-to-noise ratio. In our experiments we could only detect 248 nm photodissociation of CH_3Cl on D_2O/Cu(110) in TOF spectra for a relatively narrow range of D_2O coverages,

Both of the TOF features are the result of photoelectron transfer from the metal substrate[41] to the CH_3Br layer atop the D_2O layer. This photoelectron driven dissociation and desorption is strongly enhanced as the D_2O coverage is increased to reach one layer of adsorbed D_2O. These features then diminish as the D_2O coverage is further increased, as can be seen in the data of Fig. 2. The overall yields observed for both the photodissociation and photodesorption features are plotted in Fig. 3. The yields reach a pronounced maximum for roughly 1–1.5 ML D_2O dosed, and then decrease, roughly exponentially with a 1/e attenuation distance of 2.7 ML of D_2O. This attenuation of photoelectron driven dissociation and desorption by ultrathin water layers is consistent with earlier photodissociation findings (1/e = 2 ML) of Gilton et al.[42] as well as those of Jo and White,[43] who measured an attenuation distance of 2.7 ML for D_2O/Pt(111) for photoelectrons above the vacuum level. In the present case it is likely that the photoelectrons responsible for the observed TOF features are subvacuum level "hot" photoelectrons, as discussed below.
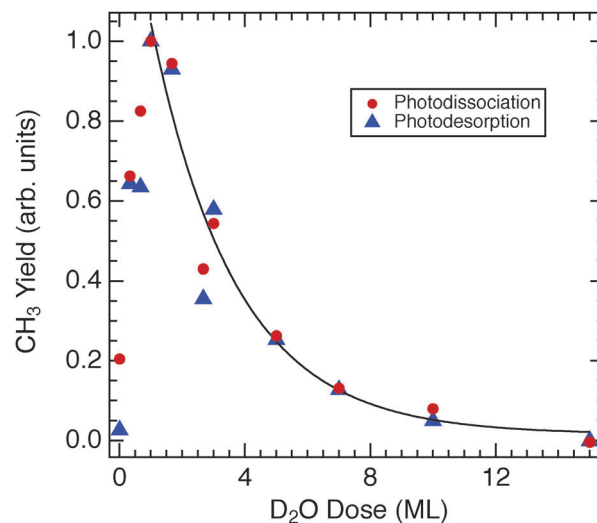

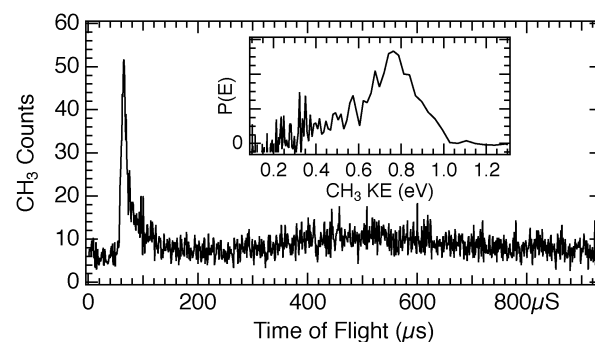Fig. 4 Time of flight spectrum from the photodissociation of 0.5 ML CH_3Cl adsorbed on 1.0 ML D_2O/Cu(110) obtained using 248 nm light. The spectrum shown is the average of three spectra, in order to improve the signal-to-noise ratio. A photodissociation feature is observed at 65 μs flight time as well as a photodesorption feature centered around 500 μs. The inset shows the same data in a CH_3 photofragment kinetic energy distribution, with a peak in P(E) near 0.75 eV.
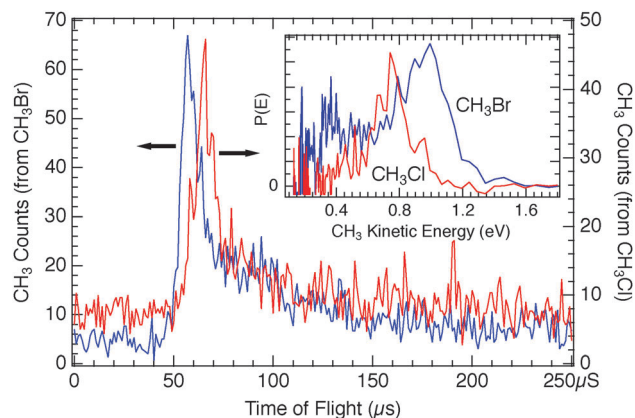
9176 | Phys. Chem. Chem. Phys., 2015, 17, 9173–9185

This journal is © the Owner Societies 2015

Fig. 5 Comparison of time-of-flight spectra from 0.5 ML CH_3Br (blue data) and CH_3Cl (red data) adsorbed on 1.0 ML $D_2O/Cu(110)$ obtained using 248 nm light. The inset plot shows this data transformed into the CH_3 fragment kinetic energy distributions.

those close to 1 ML which also gave the largest photofragment yields seen for CH_3Br in Fig. 3. For the $CH_3Cl/D_2O/Cu(110)$, the photodesorption feature near 500 μs is small relative to that that seen for CH_3Br. Detailed comparison between the 248 nm photodissociation of CH_3Cl and CH_3Br on $D_2O/Cu(110)$ is shown in Fig. 5 – the CH_3 photofragments from CH_3Cl are roughly 8 to 9 μs slower than those from CH_3Br, corresponding to roughly 0.25 eV lower translational energy. Based on the free molecule dissociation energetics for DEA from eqn (1) both the absolute and the relative CH_3 kinetic energies can be considered for the observed photodissociation of CH_3Br and CH_3Cl. The electron affinities of the halogen atoms are 3.36 eV (Br) and 3.61 eV (Cl), and the dissociation energies D_0 are 3.05 eV (CH_3–Br) and 3.63 eV (CH_3–Cl).‡[44] We do not know precise values for the energy contributions from the incident electrons or the anion solvation (E_{e^-} and ΔE_{solv} in eqn (1)), but these can be estimated. For CH_3Br condensed in a dielectric medium close to a metal surface, the dissociative anion state is shifted to lower energy[45] and results in a DEA process facilitated by very low energy electrons, close to the vacuum level. Using the estimate for electrons causing DEA of E_{e^-} = 0 eV (at the system vacuum level E_{vac}) results in ΔE_{solv} = 1.06 eV for CH_3Br, which is a reasonable value based on estimated values as well as the polarization induced shifts seen experimentally in other similar contexts.[46] It may well be the case that the maximum CH_3Br DEA cross section occurs for electrons below E_{vac}.[47,48] In the case of adsorbed CH_3Cl, it is also well-known that the anion state is shifted to much lower energy relative to the ground-state neutral[45] so that low energy electrons can cause DEA with a large cross section. Assuming E_{e^-} = 0 results in an estimate of ΔE_{solv} = 1.31 eV. This value for ΔE_{solv} appears too large in comparison with that for CH_3Br, since both anions would be expected to be in similar dielectric environments and have similar dissociation times. The value of ΔE_{solv} would be reduced if the relevant E_{e^-} for DEA is 0.25 eV larger for the

CH_3Cl than CH_3Br. This magnitude of differing incident electron energy responsible for DEA is compatible with observations in electron beam experiments on CH_3Cl and CH_3Br condensed on Kr/Pt.[45] While the magnitudes of the polarization shifts are likely different between the Kr/Pt and the $D_2O/Cu(110)$ substrates, the correspondence between the polarization shifts and the requisite incident electron energies seems to be reasonable.

3.2 Photodissociation at 193 nm on $D_2O/Cu(110)$

Irradiation using 193 nm ($h\nu$ = 6.4 eV) light for CH_3Br and CH_3Cl adsorbed on $D_2O/Cu(110)$ produced TOF spectra that display neutral photodissociation of the methyl halides in addition to the photoelectron driven dissociation seen using 248 nm light. Fig. 6 shows a TOF spectrum for 1 ML CH_3Br adsorbed on 1 ML $D_2O/Cu(110)$. Although the photon energy is 1.4 eV larger, so that a wider range of photoelectron energies is generated, the CT-DEA photodissociation feature appears at the same flight time (60 μs) and translational energy (1.0 eV) as for the 248 nm data. The 193 nm photons also produce a neutral photodissociation peak seen at 39 μs flight time, which appears at 2.1 eV in the inset photofragment kinetic energy distribution. That the neutral photodissociation is observed for CH_3Br using 193 nm light but not for 248 nm is consistent with the gas-phase neutral photodissociation cross section, being 6.0×10^{-19} cm^2 at 193 nm, and is at least two order of magnitude smaller at 248 nm.[49] Photodissociation TOF features for varying D_2O pre-coverages are shown in Fig. 7 in which similar variation in the CT-DEA dissociation is seen at 193 nm as was the case for 248 nm, while the neutral photodissociation feature is seen to increase with the initial D_2O coverage and then remains essentially constant for increasing D_2O layer thickness.

Irradiation of CH_3Cl adsorbed on $D_2O/Cu(110)$ using 193 nm light results in TOF spectra such as that shown in Fig. 8, in which both a neutral photodissociation peak (at 46 μs) and a CT-DEA driven dissociation at 62 μs are seen, as well as a small photodesorption feature centered around 500 μs. As for CH_3Br,

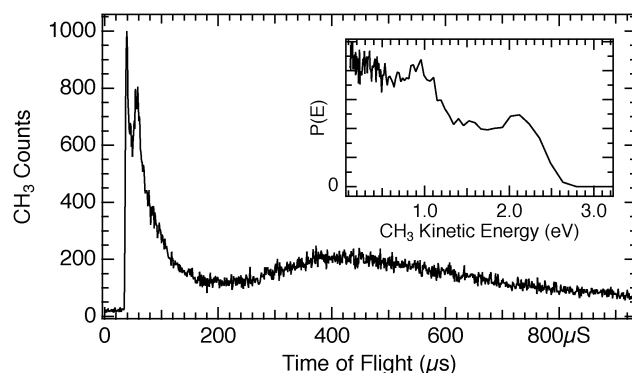**Fig. 6** Time of flight spectrum for 1 ML CH_3Br on 1 ML $D_2O/Cu(110)$ obtained using 193 nm light. As compared to Fig. 1, there is an additional photodissociation component peaking at 38 μs flight time due to neutral photodissociation of the CH_3Br. The inset data shows the distribution of CH_3 photofragment kinetic energies, with the neutral photodissociation peak at 2.1 eV and the photoelectron driven DEA feature at 1.0 eV.

‡ We have used D_0^{298} values without correction for T = 90 K of our experiment.
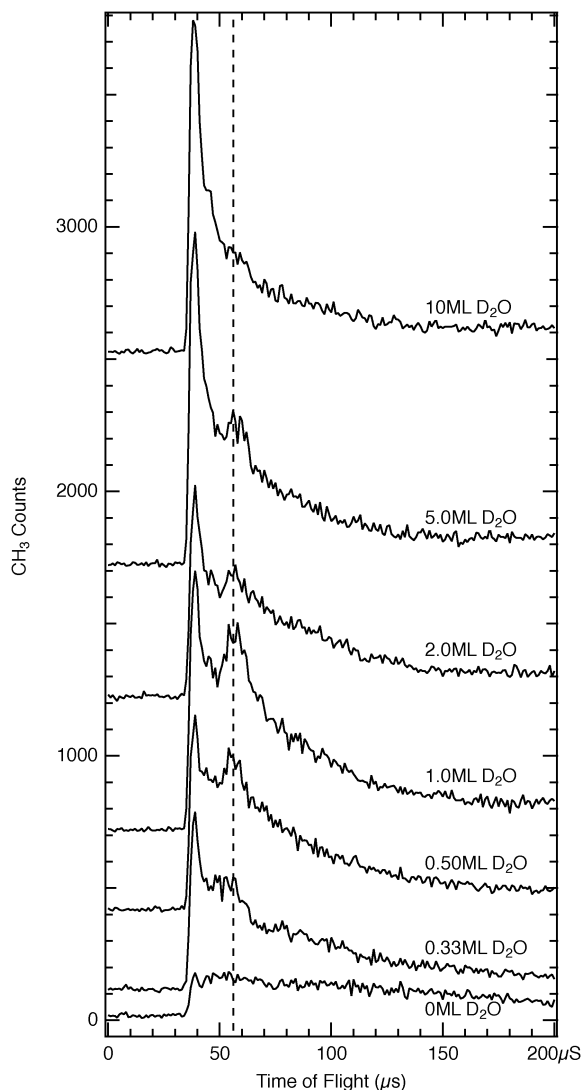

Fig. 7 Sequence of TOF spectra from 1 ML CH₃Br on D₂O/Cu(110) obtained using 193 nm light for varying amounts of D₂O coverage on the surface. The photoelectron driven photodissociation feature at 58 μs flight time grows rapidly for low D₂O coverages and then diminishes for D₂O layer thicknesses beyond 1 ML, while the neutral photodissociation feature at 38 μs grows with D₂O coverage and then remains constant for thicker D₂O layers.

Fig. 8 Time of flight spectrum from 0.7 ML CH₃Cl on 1 ML D₂O/Cu(110) obtained using 193 nm light. As compared to the same system at 248 nm (Fig. 4), an additional peak is observed at 46 μs flight time, a consequence of neutral photodissociation. The inset plot shows the data plotted to show the CH₃ kinetic energy distribution, with peaks at 0.8 eV (photoelectron DEA) and 1.5 eV (neutral photodissociation).

Fig. 9 A sequence of TOF spectra from 0.5 ML CH₃Cl adsorbed on varying amounts of D₂O on Cu(110), obtained using 193 nm light. The amplitude of the DEA feature is strongly modulated by the D₂O coverage, peaking for 1 ML of D₂O. The amplitude of the neutral photodissociation peak is relatively unaffected by the D₂O coverage, beyond a minimum amount.

the photoelectron driven photodissociation and photodesorption feature magnitudes are strongly enhanced for roughly 1 ML D₂O coverage, and diminish rapidly as the D₂O precoverage is increased above 1 ML, as shown in Fig. 9 for the photodissociation peaks. The observation of the neutral photodissociation peak of CH₃Cl at 193 nm is reasonable based on the gas-phase cross section of 0.7×10^{-19} cm², which is at least several orders larger than at 248 nm.[49] The observed relative yields from neutral photodissociation for CH₃Br and CH₃Cl at 193 nm (for example, Fig. 7 and 9) are also consistent with the relative magnitudes (∼9×) of the gas-phase cross sections at this wavelength.

3.3 Photodissociation at CH₃X on CH₃OH/Cu(110)

As a comparison and contrast to the D₂O/Cu(110) system, we have also studied the photodissociation of the same small

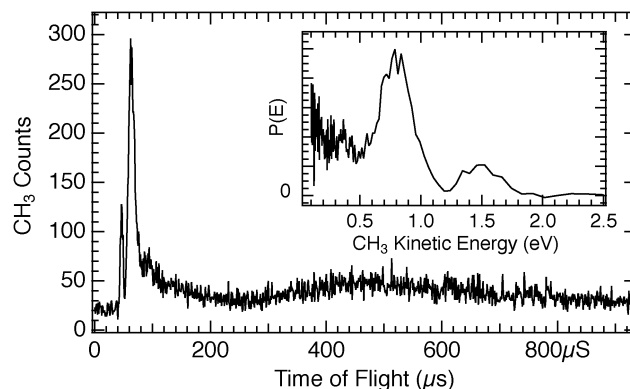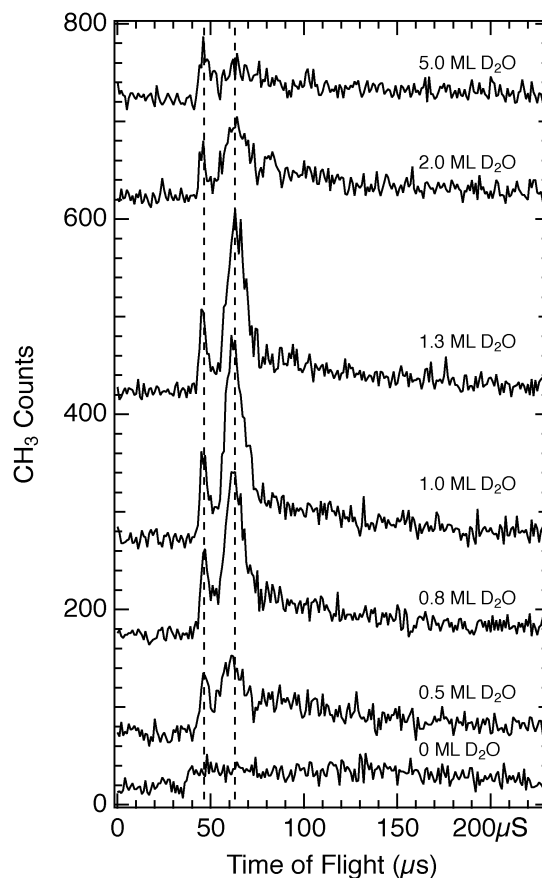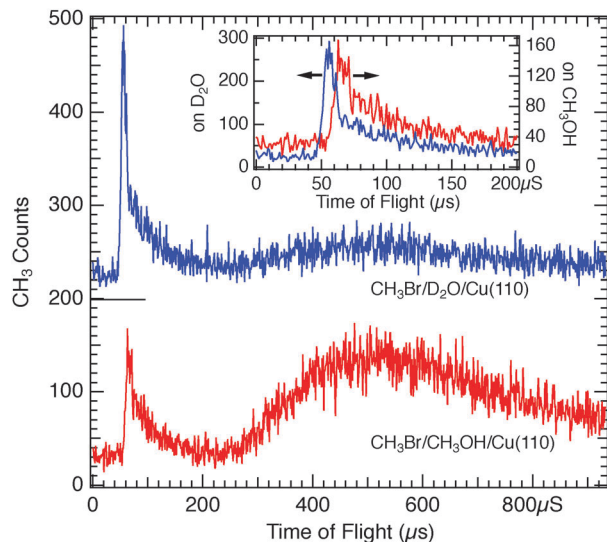halomethane molecules adsorbed on CH₃OH/Cu(110). Methanol has a similar dipole moment[44] (1.70 D) to water (1.85 D), and on Cu(110) its adsorption results in a comparable decrease in work

9178 | *Phys. Chem. Chem. Phys.*, 2015, **17**, 9173–9185

This journal is © the Owner Societies 2015

Fig. 10 Comparison of TOF spectra obtained from 0.3 ML CH_3Br adsorbed on $D_2O/Cu(110)$ (top, blue trace) with $CH_3OH/Cu(110)$ (lower, red trace), using 248 nm light. When adsorbed on CH_3OH (as compared to D_2O), the CH_3Br photodissociation feature near 60 µs flight time is reduced in magnitude but broader, whilst the photodesorption feature centered around 500 µs flight time is significantly larger in amplitude. The inset plot shows detail of the CT-DEA photodissociation feature for CH_3Br, being slower on CH_3OH as compared to on D_2O.

function ($\Delta\phi = -1.35$ eV for 1 ML at 140 K (ref. 22)) as for water ($\Delta\phi = -1.0$ eV for 1 ML (ref. 50)). In some respects our photochemical observations from CH_3OH layers are comparable to those from D_2O – the photoelectron-driven DEA processes are strongly enhanced for monolayer coverages and diminish for thicker CH_3OH layers, however the dynamics of dissociation are significantly altered. Fig. 10 shows comparative TOF spectra for CH_3Br adsorbed on $CH_3OH/Cu(110)$ and $D_2O/Cu(110)$ obtained using 248 nm light. For the $CH_3OH/Cu(110)$ substrate, the CH_3Br CT-DEA photodissociation signal is slower, reduced in magnitude and broadened, while the photodesorption signal centered around 500 µs is substantially increased. The inset plot of Fig. 10 highlights the observation that the CH_3 fragments from photoelectron driven dissociation are slower for CH_3Br/CH_3OH than those from CH_3Br on D_2O, with the leading edge of the main TOF peaks separated by ~8 µs.

Upon changing the photon energy to 193 nm, the TOF spectrum for CH_3Br adsorbed on $CH_3OH/Cu(110)$ of Fig. 11 displays both photoelectron as well as neutral photodissociation features and allows comparison with that from $D_2O/Cu(110)$. The inset plot of the CH_3 fragment kinetic energy distributions shows that the slower CH_3 photofragments seen from CT-DEA of CH_3Br/CH_3OH as compared to CH_3Br/D_2O are unique to the charge-transfer dissociation – the CH_3 photofragments from neutral photodissociation at 193 nm have the same translational energy on both molecular films.

Fig. 12 highlights another difference seen for CH_3Br adsorbed on $CH_3OH/Cu(110)$ – though using 193 nm light has a photon energy sufficient for neutral photodissociation of CH_3Br, this is not observed at low coverages of CH_3Br on CH_3OH and is seen
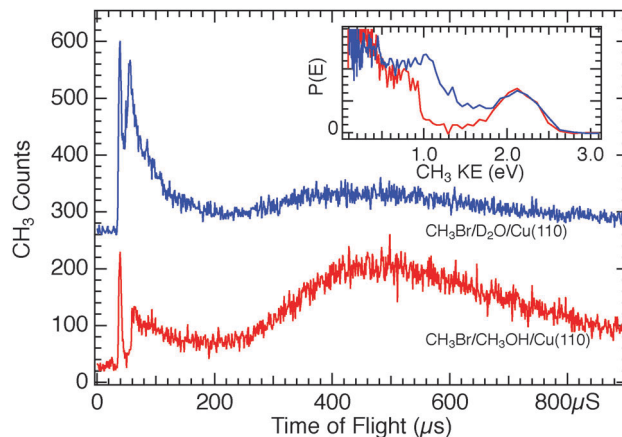
Fig. 11 Comparison of TOF spectra obtained for 0.5 ML CH_3Br adsorbed on 1 ML $D_2O/Cu(110)$ (top, blue trace) and 1.3 ML CH_3Br on $CH_3OH/Cu(110)$ (lower, red trace), using 193 nm light. The inset plot shows the same data as a function of the CH_3 fragment kinetic energy. The neutral photodissociation peak (40 µs; 2.2 eV) is the same on both substrates, while the CT-DEA photodissociation feature is observed to have lower KE on CH_3OH as compared to D_2O, as also seen at 248 nm in Fig. 10.
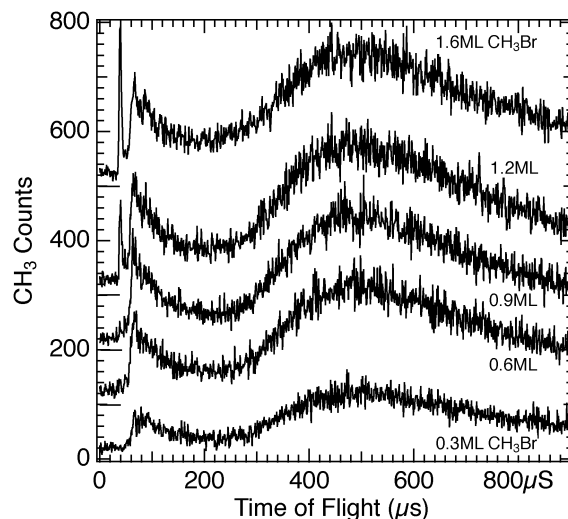
Fig. 12 A series of TOF spectra for varying amounts of CH_3Br adsorbed on 1 ML CH_3OH on Cu(110), obtained using 193 nm light. While the CT-DEA photodissociation and the photodesorption features are observed at all CH_3Br coverages, the neutral photodissociation of CH_3Br is only observed for coverages of CH_3Br above 1 ML.

only for CH_3Br coverages beyond roughly 1 ML, independent of the precoverage amount of CH_3OH. This is in contrast to the analogous situation seen for $D_2O/Cu(110)$, in which the 193 nm neutral photodissociation is not observed to have a minimum onset coverage of CH_3Br.

Based on the findings for CH_3Br on $CH_3OH/Cu(110)$, the expectations for CH_3Cl adsorbed on this substrate would be for a reduced but broadened photoelectron-driven dissociation signal and increased photodesorption. In this light, the observed TOF spectra for this system, such as that of Fig. 13 are surprising. The yield of CH_3 photofragments from photoelectron-driven dissociation is very large and also narrow in the TOF spectra
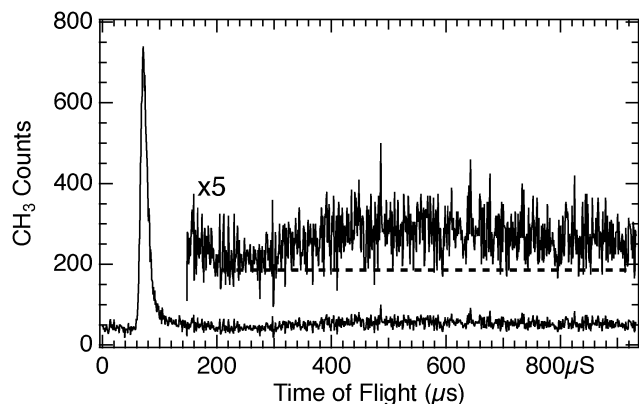
Fig. 13 Time of flight spectrum from the photodissociation of 0.3 ML CH_3Cl adsorbed on 1 ML $CH_3OH/Cu(110)$ using 248 nm light. The photo-dissociation *via* the DEA mechanism give a large yield of CH_3 photofragments (peak at 71 μs), and a very small photodesorption feature (the dashed line indicates the CH_3 background count level).
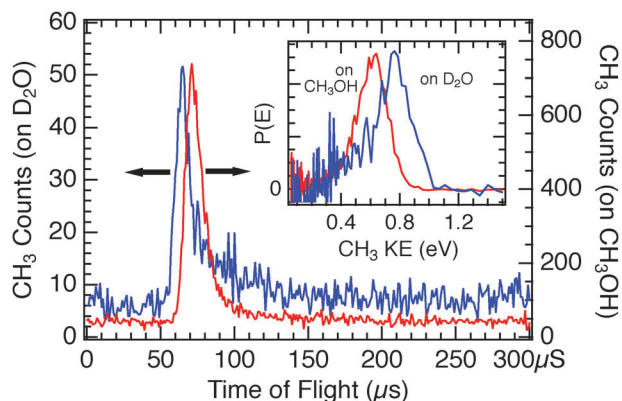

Fig. 14 Comparison of TOF spectra for CH_3Cl photodissociation at 248 nm, between that adsorbed on $D_2O/Cu(110)$ (blue trace) and on $CH_3OH/Cu(110)$ (red trace). The inset plot shows the same data plotting the probability distribution as a function of the CH_3 photofragment kinetic energy. While the yield of CH_3 photofragments is much larger for CH_3Cl adsorbed on CH_3OH (note the respective *y*-axis scales for the TOF spectra), the kinetic energy release is smaller than when adsorbed on $D_2O/Cu(110)$.

compared to the analogous case for CH_3Br, and the photo-desorption feature is much smaller than that seen in the previously described systems. In common with the findings for CH_3Br, the CT-DEA photodissociation peak for CH_3Cl on $CH_3OH/Cu(110)$ is at a longer flight time than seen for $D_2O/Cu(110)$, as shown in Fig. 14. As compared to the D_2O case, the CH_3 photofragments from CH_3Cl photodissociation are ∼6 μs slower, or as shown in the inset plot of Fig. 14, the peak in the $P(E)$ distribution is at 0.15 eV lower kinetic energy.

That the observed photodissociation for CH_3Cl on $CH_3OH/Cu(110)$ is photoelectron driven is supported by data such as that shown in Fig. 15, in which the amount of CH_3OH is varied for a fixed CH_3Cl dose. The photodissociation yield is found to increase dramatically from that of the clean surface, to a maximum yield found for roughly 1 ML CH_3OH. The yield is then observed to decrease, and a simple exponential fit

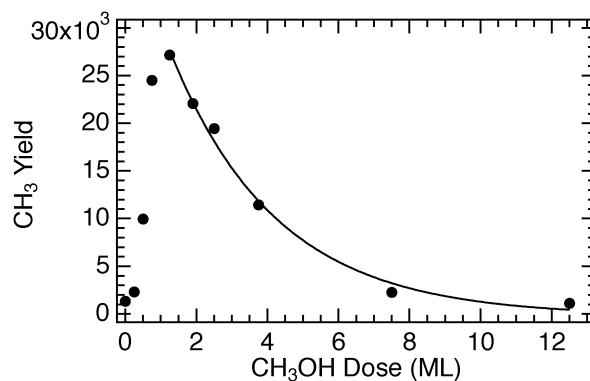**Fig. 15** Yield of CH_3 photofragments from photodissociation of $CH_3Cl/CH_3OH/Cu(110)$ as the CH_3OH coverage is varied. The data is obtained using 193 nm light and 1 ML of CH_3Cl. The solid line is a simple exponential fit to the data points above 1 ML CH_3OH coverage, and represents a 1/e attenuation distance of 3.0 ML for CH_3OH.

suggests an attenuation length of 3.0 ML for the relevant photoelectron transport through CH_3OH, which is comparable to the 2.7 ML discussed above for D_2O. Similar variations with CH_3OH dose are also found for CH_3Br/CH_3OH for the photo-electron driven photodissociation peak as well as for the photodesorption feature. The neutral photodissociation peak for CH_3Br seen at 193 nm (the TOF peak at 39 μs in Fig. 12) behaves differently – increasing monotonically with for low CH_3OH doses and remaining essentially constant for higher multilayer doses. As the CH_3Cl coverage is increased for a fixed amount (1 ML) of CH_3OH, the CH_3 photoyield due to photoelectron driven dissociation grows monotonically with the CH_3Cl dose until 1 ML is dosed, and then remain essentially fixed for higher doses. We interpret this result as being due to having only the first monolayer of CH_3Cl able to stick to the $CH_3OH/Cu(110)$ substrate at the temperature used for our experiments.

It is also notable that the CH_3 photofragment translational energy distribution from DEA does not change as the CH_3OH thickness is varied nor over the range of wavelengths that $CH_3Cl/CH_3OH/Cu(110)$ photodissociation is observed (308 nm to 193 nm) – TOF spectra from different wavelengths can be overlaid and aside from simple linear scaling, are otherwise identical. This also appears to be the case in our data for the CH_3Br on $D_2O/Cu(110)$ and $CH_3OH/Cu(110)$, though the distributions are more complex. This point is salient as photo-dissociation *via* DEA is often interpreted in terms of the '3-step model'[32,51] in which the energy available for dissociation should reflect the convolution of the photoelectron distribution with the anion resonance attachment energy distribution. This leads to an expectation for lower energy available (eqn (1)) at the red end of the wavelengths used for photodissociation that should be reflected as a suppression of the high-energy side CH_3 translational energy distributions, but this is not observed. One possible explanation for this lack of correlation between photon energy and fragment translational energy could be that intermediate electron sates modify the density of states at the vacuum interface, such as image-potential derived states[15] that couple with the anion attachment resonance.[52]

9180 | *Phys. Chem. Chem. Phys.*, 2015, **17**, 9173–9185

This journal is © the Owner Societies 2015

A striking observation for CH$_3$Cl/CH$_3$OH/Cu(110) at 193 nm is that we do not observe CH$_3$ photofragments from neutral photodissociation of the CH$_3$Cl at 193 nm under any of the conditions studied – data obtained at 193 nm is essentially identical to that from 248 nm as shown in Fig. 13. Given the cross sections and intensities measured for CH$_3$Cl/D$_2$O/Cu(110) (e.g. Fig. 9), the neutral photodissociation channel should be easily observable. The absence of neutral photodissociation in the TOF spectra from the first monolayer of CH$_3$Br on CH$_3$OH/Cu(110) that is seen in Fig. 12 indicates that the neutral photodissociation mechanism is suppressed at 193 nm for CH$_3$Cl and CH$_3$Br on the CH$_3$OH/Cu(110) substrate. This observation is discussed further in Section 4.

As described above, we see altered kinetic energy distributions for the CH$_3$ photofragments via CT-DEA for CH$_3$X on CH$_3$OH as compared to D$_2$O. We have also directly compared the observed distributions for CH$_3$Cl to those of CH$_3$Br adsorbed on CH$_3$OH, which are shown in Fig. 16 for 248 nm light. The CH$_3$ photofragments from CT-DEA of CH$_3$Br are slightly faster than those from CH$_3$Cl in the onset of the distribution as well as the most probable time. As shown in the inset plot, the leading edge of the P(E) distribution is at 0.20 eV higher energy for the CH$_3$Br as compared to that of CH$_3$Cl. This is a smaller kinetic energy difference than was seen for these two molecules on D$_2$O in Fig. 5 ($\sim$0.3 eV). This smaller difference in kinetic energies is a result of the larger downward shift in CH$_3$ fragment kinetic energy for CH$_3$Br on CH$_3$OH as compared to D$_2$O ($\Delta T_{CH_3} = -0.20$ eV) as compared to that for CH$_3$Cl ($\Delta T_{CH_3} = -0.15$ eV).

3.4 Cross sections

We have measured depletion cross sections for a selection of the molecular thin films examined in this work. These cross sections are obtained by recording CH$_3$ photofragment yields from photodissociation and/or photodesorption for a sequence

Fig. 16 Comparison of the 248 nm photodissociation of CH$_3$Br (blue trace) and CH$_3$Cl (red trace) adsorbed on 1 ML CH$_3$OH/Cu(110). The inset plot shows the related probability distributions as a function of the CH$_3$ fragment translational energy.

Table 1 Observed depletion cross sections based on observed photo-dissociation and photodesorption yields from CH$_3$X on different mono-layer films on Cu(110), and gas-phase photodissociation cross section.[49] Entries indicated by '>0' have detectable yields but insufficient signal to measure a reliable cross section. Entries indicated by a dash '—' had no detectable photochemical signal in the TOF spectra. The value in brackets for CH$_3$Br/D$_2$O at 193 nm is that from a multilayer D$_2$O film

λ (nm) [$h\nu$ (eV)]	Depletion cross section ($\times 10^{-18}$ cm^2)					
	CH$_3$Br/ D$_2$O	CH$_3$Br/ CH$_3$OH	CH$_3$Cl/ D$_2$O	CH$_3$Cl/ CH$_3$OH	CH$_3$Br (gas)[49]	CH$_3$Cl (gas)[49]
193 [6.42]	1.9(0.92)	2.5	0.55	3.4	0.56	0.070
248 [5.00]	0.45	0.93	>0	0.77	0.015	—
308 [4.02]	0.40	>0	>0	0.71	—	—
351 [3.53]	>0	—	—	—	—	—

of TOF spectra. Time-of-flight spectra are obtained using 200–300 laser pulses per scan, then repeated for 10 or more successive scans. In the systems studied here, the TOF signals are observed to diminish as the net laser photon flux was increased, and the resulting yield vs. flux curves could be fit by a simple exponential decay model. Reasonable fits to the data were obtained, at least in the low flux limit, though this does not exclude the possibility that more complex photo-chemical processes not seen in the TOF data might be occur-ring in these heterogeneous thin films. In the cases where multiple features are observed in the TOF spectra (neutral photodissociation, DEA, photodesorption) we measured sepa-rate depletion cross sections for each feature. In the cases we examined, we measured the same (within experimental error) cross sections for co-present features. The resulting extracted cross sections are reported in Table 1. The values reported are nearly all obtained using 1 ML of the D$_2$O or CH$_3$OH, with between 0.5 and 1 ML of the methyl halide adsorbed on top. The one exception is for the λ = 193 nm photodissociation of CH$_3$Br/D$_2$O in which we also report the value for 15 ML of D$_2$O (value in brackets) which represents the cross section in which only neutral photodissociation is observed in the TOF spectra. This value of 9.2×10^{-19} cm^2 is somewhat larger than that reported for gas-phase[49] CH$_3$Br ($\sigma = 6 \times 10^{-19}$ cm^2). This discrepancy may well be due to the rather large error associated with the absolute cross sections we estimate ($\pm$50%).§ In several cases we can observe and identify the photochemical processes in the TOF spectra (and some of these are shown and discussed above) but the yields are too low to yield a reliable cross section estimate, so these are denoted by '>0'. Situations in which no photochemical signals could be discerned in the TOF spectra are denoted by '—'. The tabulated values highlight an interesting contrast between the CH$_3$Br and CH$_3$Cl
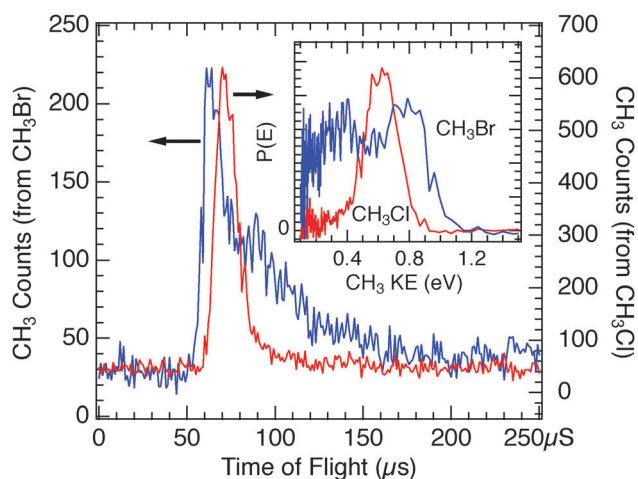
§ Various geometrical factors as well as the variable laser beam profile uniformity lead to this large absolute error. At a given wavelength, the relative errors of our cross section estimates are quite small – we typically measured cross sections for different molecular combinations on the same day without modifying the laser geometry and using the same laser gas fill, so that the sources of most relative errors are small (<10%) for these values. We do expect that our absolute cross section values and those for comparing values at two different wavelengths have larger errors.

photodissociation results – the CH_3Br photodissociation is observed at longer wavelengths on the $D_2O/Cu(110)$ films, while for CH_3Cl, the photodissociation is larger and seen at longer wavelengths on the $CH_3OH/Cu(110)$ films. We are not aware of any previous observations of CH_3Cl photodissociation with substantial cross section for $\lambda = 308$ nm (4.02 eV) photons. There are few previously reported photochemical cross-sections for halomethanes co-adsorbed with D_2O or CH_3OH. A study of CD_3Cl caged within H_2O layers on Ru(100) measured cross sections of $\sim 0.5 \times 10^{-18}$ cm^2 at 193 nm and $\sim 0.02 \times 10^{-18}$ cm^2 at 248 nm by observation of CD_3Cl depletion,[53] values that are compatible with those reported for $CH_3Cl/D_2O/Cu(110)$ in Table 1.

3.5 Angular distributions

The substantive differences observed in the photodissociation dynamics between CH_3Br and CH_3Cl when adsorbed on $CH_3OH/Cu(110)$ were further investigated by measurements of the angular variation of the signals. For $CH_3Cl/CH_3OH/Cu(110)$ we found an angular distribution for the CH_3 photofragments well fit by a $\cos^N \theta$ functional form with $N = 4$, which does not change substantially with CH_3Cl coverage. As the detection angle from the surface normal increases, the CH_3 photofragment kinetic energy distribution is hardly affected, as seen in Fig. 17. There is a small diminution of the fastest CH_3 fragments at larger escape angles, but no increase in the proportion of the lower energy inelastic tail even for the $60°$ detection angle. In contrast, the TOF spectra for CH_3Br photodissociation (e.g. Fig. 11) show clear evidence of inelastic interactions on both the $D_2O/Cu(110)$ and $CH_3OH/Cu(110)$ surfaces. The $P(E)$ distributions for a range of detection angles shown in Fig. 18 for $CH_3Br/D_2O/Cu(110)$ display a more pronounced inelastic tail for CH_3 kinetic energies lower than that of the main CT-DEA peak, and in some spectra a peak can be discerned near $T_{CH_3} \approx 0.4$ eV (e.g. insets in Fig. 5 and 16). We ascribed a similar feature seen for $CH_3I/D_2O/Cu(110)$ to chattering as downward pointing CH_3 fragments interact with the substrate before escaping.[28] The inelastic signals are seen to grow in relative size as the detection angle from the surface normal is increased. The angular distributions of the CH_3 photofragments from CH_3Br are peaked in the surface normal direction ($\propto \cos^N(\theta)$ with $N = 4$–5) but also display a shift to lower kinetic energy in both the fastest CH_3 photofragments as well as the larger 'inelastic tail' as the angle increases.

4 Additional discussion

4.1 Structure and dynamics

In many respects the structural properties of the halomethanes are quite similar, with the structure of the solids dominated by the electrostatic dipole interactions (dipole moments: CH_3Cl-1.90 D; CH_3Br-1.82 D; CH_3I-1.64 D).[44] In the bulk solid, although the molecular ordering is dominated by dipolar interactions, there are distinct differences between the structure of crystalline CH_3Cl[54] and CH_3Br,[55] which is ascribed to

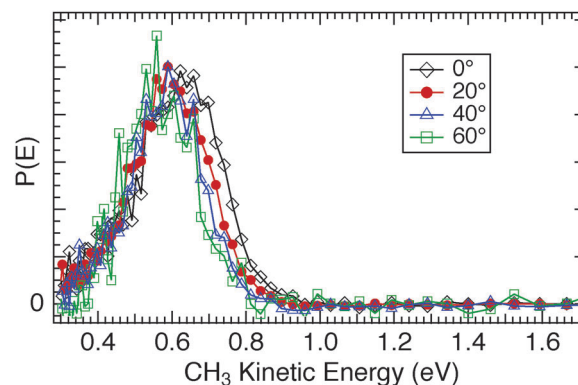**Fig. 17** Comparison of the CH_3 photofragment translational kinetic energy distributions from 248 nm photodissociation of CH_3Cl adsorbed on 1 ML $CH_3OH/Cu(110)$ as a function of detection angle from the surface normal.
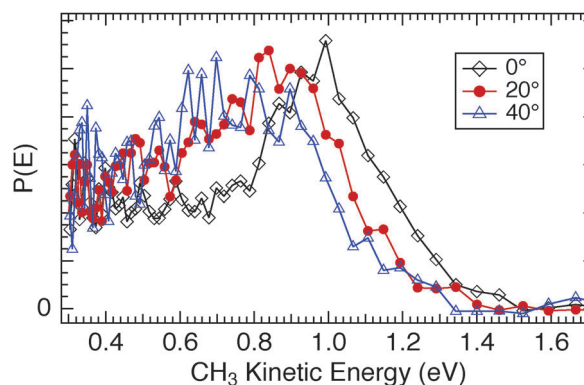

Fig. 18 Comparison of the CH_3 photofragment probability distributions from 248 nm photodissociation of CH_3Br adsorbed on 1 ML $D_2O/Cu(110)$ as a function of detection angle from the surface normal.

differences in the halogen–halogen binding interactions.[55] The observed photochemical dynamics for CH_3Br and CH_3Cl on $D_2O/Cu(110)$ do not indicate significant differences in the structural aspects that impact the observed dynamics. For both methyl halides, we observe CT-DEA on thin D_2O films over a range of wavelengths in which hot photoelectrons of the appropriate energies would be generated. In addition we observe photodesorption of the intact CH_3X molecules that correlate with the CT-DEA dissociation fluxes. The observed dynamics are compatible with an antiferroelectric structure for the methyl halides, and given the net repulsive interactions with the D_2O, it is anticipated that CH_3X islands are present even at low coverages. These observations are consistent with our previous study of $CH_3I/D_2O/Cu(110)$.[28] At the shorter 193 nm wavelength, we also observe neutral photodissociation of both CH_3Br and CH_3Cl, with apparent cross sections comparable to those for the gas-phase. That these neutral photodissociation TOF features are very well-defined indicates that the measured CH_3 photofragments are from 'CH$_3$-up' oriented molecules that do not significantly interact with the surface during or post bond-cleavage.

The clean Cu(110) substrate has a work function of 4.48 eV,[44] and the D_2O and CH_3OH adlayers reduce the work function by

9182 | *Phys. Chem. Chem. Phys.*, 2015, **17**, 9173–9185

This journal is © the Owner Societies 2015

1 eV or more for monolayer coverages.[22,50] In addition, the CH_3X adlayers are known to reduce the work function on D_2O[25,26] due to the preferred orientation of the dipole. Hence even for the longest wavelength (351 nm, $h\nu$ = 3.51 eV) used in this work, we expect that free photoelectrons (i.e. above the vacuum level) are present under most conditions studied, in addition to the subvacuum level 'hot' photoelectrons. At λ = 351 nm we only observed photoelectron-driven dissociation and photodesorption in the TOF spectra for the $CH_3Br/D_2O/Cu(110)$ and $CH_3I/D_2O/Cu(110)$ systems. Photodissociation was observed for a narrow range of D_2O coverages around 1 ML, where the work function minimum and maximum CH_3 yields (e.g. Fig. 3) are found. Since we observe no photoelectron-driven dissociation of CH_3Cl on either $D_2O/Cu(110)$ or $CH_3OH/Cu(110)$ using 351 nm light, it can be concluded that higher energy photoelectrons are required for DEA of CH_3Cl than are substantially available. Upon increasing the photon energy by 0.49 eV using 308 nm light (and consequently producing a similarly increased range of photoelectron energies), we observe not only much stronger dissociation signals from $CH_3Br/D_2O/Cu(110)$ but also photo-dissociation of $CH_3Cl/CH_3OH/Cu(110)$. This indicates a threshold photon energy between 3.53 eV and 4.02 eV for the latter system. The contrasting behaviour of CH_3Br and CH_3Cl photo-dissociation yields on $D_2O/Cu(110)$ and $CH_3OH/Cu(110)$ are highlighted near these thresholds. The CT-DEA photodissociation of CH_3Cl is most prominent on the $CH_3OH/Cu(110)$ surface, and is only observed at shorter wavelengths on $D_2O/Cu(110)$ and with lower CH_3 photofragment yields and cross-section. In contrast the CH_3Br CT-DEA photodissociation is more prominent on the $D_2O/Cu(110)$, and we did not observe CH_3 photo-fragments or photodesorption on $CH_3OH/Cu(110)$ using 351 nm light. We believe that these observations are related to the differing molecular structures of CH_3Br and CH_3Cl on the CH_3OH and D_2O molecular interfaces.

Further evidence for differing molecular ordering of CH_3Br and CH_3Cl on the two substrates considered comes from the observed CH_3 time-of-flight distributions. The TOF spectra from $CH_3Cl/CH_3OH/Cu(110)$ display a single narrow features due to CT-DEA of the CH_3Cl ($\bar{E}$ = 0.62 eV, ΔE = 0.24 eV FWHM). This system displays almost no 'inelastic tail' of lower energy CH_3 photofragments (E_{trans} < 0.4 eV, see Fig. 16 and 17) and there is only a very small photodesorption feature as compared to the other systems studied in this work. These observations for $CH_3Cl/CH_3OH/Cu(110)$ lead us to propose that the CH_3Cl molecules are adsorbed primarily with the $Cl-CH_3$ axis normal to the surface and in the 'CH_3-up' orientation. Bond-breaking due to DEA leads to the departing CH_3 photofragment having little opportunity for inelastic interactions as it departs the surface and hence a relatively narrow translational energy distribution. Due to the solvation shift of the anion, the dissociation probability is high (i.e. low autoionization or quenching prob-ability) so there is a relatively low probability for excited CH_3Cl that do not dissociate but might have sufficient energy to break the molecule–surface bond and contribute to photodesorption. On the $D_2O/Cu(110)$ surface the photodissociation of CH_3Cl yields fewer CH_3 photofragments and a significantly lower cross

section (Table 1). The data such as in Fig. 4, 8 and 14 show that there is a similarly small inelastic tail (E_{trans} < 0.5 eV) and a somewhat larger photodesorption signal as compared to the situation on $CH_3OH/Cu(110)$. An IR-SFG study of CH_3Cl on $D_2O/Pd(111)$ indicates that the $Cl-CH_3$ bond is along the surface normal in the 'CH_3-up' orientation,[26] and our own observations of the angular distributions for CH_3 photofragments on both CH_3OH and D_2O are in accord with this. Depending on the dosing order and amount,[25] it is possible that some mixed orientations for CH_3Cl on D_2O can be formed. We do believe that the $CH_3Cl/D_2O/Cu(110)$ TOF data shows evidence for a minor amount antiferroelectric ordering of the CH_3Cl – that downward pointing CH_3 photofragments will inelastically scatter from the surface to contribute to the inelastic tail, and that 'chattering' type interactions will also lead to more quenching and subsequent molecular photodesorption[56] on $D_2O/Cu(110)$ than for $CH_3OH/Cu(110)$.

On the basis of the observed energy and angular distribu-tions, we conclude that CH_3Br on the $D_2O/Cu(110)$ and $CH_3OH/Cu(110)$ substrates has a more mixed orientational ordering than for CH_3Cl, most likely an antiferroelectric structure with both 'Br-up' and 'Br-down' configurations, though to a lesser extent on $D_2O/Cu(110)$ than for $CH_3OH/Cu(110)$. The role of local work function modulated by the ordering of surface dipoles at the interface has been noted previously,[47,57] and in the case of $CH_3OH/Cu(110)$, the preponderance of 'CH_3-up' ordering of the CH_3Cl lowers the barrier for photoelectron interactions to a larger extent than the mixed ordering of the CH_3Br. In an analysis of CH_3Br electron- and photodissociation on Ru surfaces it was found that the 'Br-down' configuration largely results in photodissociation while the 'Br-up' configu-ration leads to photodesorption.[56] We also see that there are differences in the solvation of CH_3Br and CH_3Cl anion states on the two substrates considered, as both are found to have lower CH_3 kinetic energies on $CH_3OH/Cu(110)$ but with a larger downward energy shift for CH_3Br. Based on eqn (1) this indicates that the dissociating CH_3Br anion is less well solvated than CH_3Cl on the CH_3OH, which could be due to differences in the orientational structure as discussed above, or could be due to steric hindrance for the larger neutral CH_3Br precursor.

There has been less previous work for the CH_3OH thin films, but FT-IR spectroscopy indicates that the equilibrium structure for $CH_3OH/Cu(110)$ at low temperatures has the O–H group close to parallel to the surface, with the CH_3 group oriented toward the surface normal.[40] This is responsible for the sign and magnitude of the surface dipole and the related change in work function that has been observed. This surface dipole struc-ture would most likely cause the preferential orientation of the halomethanes in a similar manner as for the $D_2O/Cu(110)$ case.

4.2 Neutral photodissociation and quenching

The neutral photodissociation of CH_3Br and CH_3Cl in the gas-phase at 193 nm has been well-studied[33–35] and occurs with rapid C–X bond scission via a set of excited states referred to as the 'A-band'. In many respects this photodissociation is similar to that of CH_3I at 248 nm, and we recently reported[28] on the

248 nm photodissociation of $CH_3I/D_2O/Cu(110)$ in which neutral photodissociation was prominent, and was identifiable for D_2O films from monolayer to many multilayers in thickness. For both CH_3Br and CH_3Cl on $D_2O/Cu(110)$ we do identify the neutral photodissociation pathway using $\lambda = 193$ nm light from the characteristic CH_3 kinetic energy distributions. When these molecules are adsorbed on $CH_3OH/Cu(110)$ however the situation is dramatically different. We do not observe neutral photodissociation of CH_3Cl, and neutral photodissociation of CH_3Br is not observed for submonolayer CH_3Br coverages. We have also examined the 248 nm photodissociation of $CH_3I/CH_3OH/Cu(110)$ over a range of conditions (e.g. Fig. 19) and do indeed observe characteristic TOF features that can only be a consequence of neutral photodissociation. While in many other respects the behaviour of CH_3I on $CH_3OH/Cu(110)$ was found to be similar to that of CH_3Br, the quenching of neutral photodissociation seen for CH_3Br and CH_3Cl at 193 nm is absent for the CH_3I at 248 nm. In the absence of any detailed calculations for the ground and excited state energy levels of the $CH_3X/CH_3OH/Cu(110)$ system, it is difficult to pin down the precise mechanism by which the excitations are quenched. We can exclude mechanisms such as orientational or steric blocking on the basis of the observed CT-DEA dissociation dynamics of the CH_3X on the same substrate, which is not similarly hindered. It is apparent that an efficient quenching due to a Dexter energy transfer (DET) mechanism is present for CH_3Br and CH_3Cl using 193 nm photoexcitation.

Solid methanol has a bandgap of 6.7 eV, and UPS study of $CH_3OH/Cu(110)$[22] places the HOMO $2a''$ level 5.5 eV below E_F, while for $H_2O/Cu(110)$ the HOMO $1b_1$ level is located 6.8–7.2 eV below E_F.[20] As for the methyl halides, a study of $CH_3X/Ag(111)$ using UPS placed the halomethane HOMO at 6.0 eV below E_F for $CH_3Cl/Ag(111)$, and at 5.4 eV and 4.4 eV respectively for CH_3Br and CH_3I monolayers on the same substrate.[58] The other ingredient required for DET is wavefunction overlap, and based on isolated molecule wavefunctions the HOMO of CH_3OH has more weight on the CH_3 group than the $1b_1$ level of D_2O does on its free D, and so is consistent with this requirement. It is of note that in CH_3OH/TiO_2 photochemistry, it has been remarked in several studies[18,59] that the CH_3OH is an effective 'hole

getter' as compared to H_2O/TiO_2. This is attractive explanation since the neutral excited state and the DEA anion state both correspond to an excess electron in the CH_3X LUMO, so the differences between these two dissociative processes are largely restricted to the differences in time that the excited state lies above the corresponding ground state prior to curve-crossing and the presence of the valence hole for the neutral excitation. However it is unclear if the quenching of the excited state hole for CH_3X by CH_3OH can be rapid enough to compete with the very rapid bond scission in CH_3X A-band photodissociation. We are not aware of similar inter-molecular quenching of rapidly dissociative neutral photoexcitation having been previously identified in the surface photochemistry literature. A somewhat similar quenching mechanism has been identified in X-ray absorption studies of homomolecular clusters of CH_3Br,[60] although in this case the $3d \rightarrow 4a_1$ core–valence excitation has dissociation competing with Auger decay, and the quenching observed in clusters is ascribed to delocalization of the CH_3Br LUMO, rather than the HOMO implicated in the present work.

Acknowledgements

References

1 G. M. Muñoz Caro and W. A. Schutte, *Astron. Astrophys.*, 2003, **412**, 121–132.

2 K. I. Öberg, R. T. Garrod, E. F. van Dishoeck and H. Linnartz, *Astron. Astrophys.*, 2009, **504**, 891–913.

3 K. I. Öberg, E. F. van Dishoeck, H. Linnartz and S. Andersson, *Astrophys. J.*, 2010, **718**, 832–840.

4 N. G. Petrik, R. J. Monckton, S. P. K. Koehler and G. A. Kimmel, *J. Chem. Phys.*, 2014, **140**, 204710.

5 Q.-B. Lu, *Phys. Rep.*, 2010, **487**, 141–167.

6 A. Bumajdad and M. Madkour, *Phys. Chem. Chem. Phys.*, 2014, **16**, 7146.

7 B. C. Garrett, D. A. Dixon, D. M. Camaioni, D. M. Chipman, M. A. Johnson, C. D. Jonah, G. A. Kimmel, J. H. Miller, T. N. Rescigno, P. J. Rossky, S. S. Xantheas, S. D. Colson, A. H. Laufer, D. Ray, P. F. Barbara, D. M. Bartels, K. H. Becker, H. Bowen, S. E. Bradforth, I. Carmichael, J. V. Coe, L. R. Corrales, J. P. Cowin, M. Dupuis, K. B. Eisenthal, J. A. Franz, M. S. Gutowski, K. D. Jordan, B. D. Kay, J. A. LaVerne, S. V. Lymar, T. E. Madey, C. W. McCurdy, D. Meisel, S. Mukamel, A. R. Nilsson, T. M. Orlando, N. G. Petrik, S. M. Pimblott, J. R. Rustad, G. K. Schenter, S. J. Singer, A. Tokmakoff, L. S. Wang, C. Wittig and T. S. Zwier, *Chem. Rev.*, 2005, **105**, 355–389.
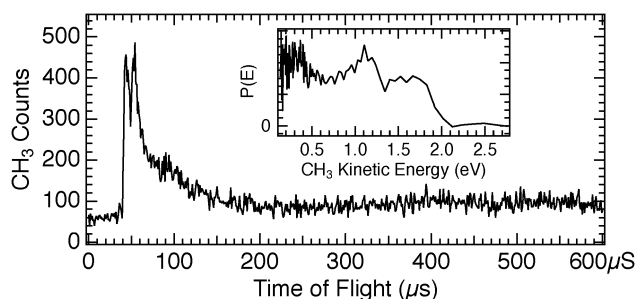
Fig. 19 Time of flight spectrum for CH_3 photofragments from 1 ML of CH_3I adsorbed on a thick (≈ 10 ML) film of CH_3OH on Cu(110) obtained using 248 nm light. The prominent peaks at 44 μs and 54 μs flight times are characteristic of the neutral photodissociation pathways for CH_3I in the A-band.

9184 | *Phys. Chem. Chem. Phys.*, 2015, **17**, 9173–9185

This journal is © the Owner Societies 2015

8 Y.-P. Kuo, H.-C. Lu, Y.-J. Wu, B.-M. Cheng and J. F. Ogilvie, *Chem. Phys. Lett.*, 2007, **447**, 168–174.

9 M. Denk, M. Hohage, L. D. Sun, P. Zeppenfeld, N. Esser and C. Cobet, *Surf. Sci.*, 2014, **627**, 16–22.

10 J. Stähler, U. Bovensiepen, M. Meyer and M. Wolf, *Chem. Soc. Rev.*, 2008, **37**, 2180–2190.

11 Q.-B. Lu and L. Sanche, *J. Chem. Phys.*, 2004, **120**, 2434–2438.

12 U. Bovensiepen, C. Gahl, J. Stähler, M. Bockstedte, M. Meyer, F. Baletto, S. Scandolo, X.-Y. Zhu, A. Rubio and M. Wolf, *J. Phys. Chem. C*, 2009, **113**, 979–988.

13 S. Ryu, J. Chang, H. Kwon and S. K. Kim, *J. Am. Chem. Soc.*, 2006, **128**, 3500–3501.

14 M. Bertin, M. Meyer, J. Stähler, C. Gahl, M. Wolf and U. Bovensiepen, *Faraday Discuss.*, 2009, **141**, 293–307.

15 S. H. Liu, A. D. Miller, K. J. Gaffney, S. Garrett-Roe, I. Bezel and C. Harris, *J. Phys. Chem. B*, 2002, **106**, 12908–12915.

16 A. D. Miller, I. Bezel, K. J. Gaffney, S. Garrett-Roe, S. H. Liu, P. Szymanski and C. B. Harris, *Science*, 2002, **297**, 1163–1166.

17 J. Zhao, B. Li, K. Onda, M. Feng and H. Petek, *Chem. Rev.*, 2006, **106**, 4402–4427.

18 Y. Tamaki, A. Furube, M. Murai, K. Hara, R. Katoh and M. Tachiya, *J. Am. Chem. Soc.*, 2006, **128**, 416–417.

19 X.-L. Zhou, X.-Y. Zhu and J. M. White, *Surf. Sci. Rep.*, 1991, **13**, 73–220.

20 M. A. Henderson, *Surf. Sci. Rep.*, 2002, **46**, 1–308.

21 A. Hodgson and S. Haq, *Surf. Sci. Rep.*, 2009, **64**, 381–451.

22 M. Bowker and R. J. Madix, *Surf. Sci.*, 1980, **95**, 190–206.

23 C. Ammon, A. Bayer, G. Held, B. Richter, T. Schmidt and H.-P. Steinrück, *Surf. Sci.*, 2002, **507**, 845–850.

24 B. L. Maschhoff, M. J. Ledema, M. Kwini and J. P. Cowin, *Surf. Sci.*, 1996, **359**, 253–268.

25 Y. Lilach and M. Asscher, *J. Chem. Phys.*, 2002, **117**, 6730–6737.

26 F. Fournier, H. Dubost, S. Carrez, W. Zheng and B. Bourguignon, *J. Chem. Phys.*, 2005, **123**, 184705.

27 S. K. Jo and J. M. White, *Surf. Sci.*, 1991, **255**, 321–326.

28 E. R. Miller, G. D. Muirhead and E. T. Jensen, *J. Chem. Phys.*, 2013, **138**, 084702.

29 A. J. DeSimone, B. O. Olanrewaju, G. A. Grieves and T. M. Orlando, *J. Chem. Phys.*, 2013, **138**, 084703.

30 Z. J. Sun, A. L. Schwaner and J. M. White, *J. Chem. Phys.*, 1995, **103**, 4279–4291.

31 D. Marinica, D. Teillet-Billy, J. Gauyacq, M. Michaud and L. Sanche, *Phys. Rev. B: Condens. Matter Mater. Phys.*, 2001, **64**, 085408.

32 F. Weik, A. de Meijere and E. Hasselbrink, *J. Chem. Phys.*, 1993, **99**, 682–694.

33 T. Gougousi, P. C. Samartzis and T. N. Kitsopoulos, *J. Chem. Phys.*, 1998, **108**, 5742–5746.

34 F. Wang, M. L. Lipciuc, A. Kartakoullis, P. Glodic, P. C. Samartzis, X. Yangand and T. N. Kitsopoulos, *Phys. Chem. Chem. Phys.*, 2014, **16**, 599–606.

35 D. Townsend, S. K. Lee and A. G. Suits, *J. Phys. Chem. A*, 2004, **108**, 8106–8114.

36 F. M. Zimmermann and W. Ho, *Surf. Sci. Rep.*, 1995, **22**, 127–247.

37 X.-L. Zhou and J. M. White, Photodissociation and Photoreaction of Molecules Attached to Metal Surfaces, in *Laser Spectroscopy and Photochemistry on Metal Surfaces: Part II*, ed. H.-L. Dai and W. Ho, World Scientific, 1995, p. 1173.

38 E. T. Jensen, *J. Chem. Phys.*, 2005, **123**, 204709.

39 G. L. Fisher and C. A. Meserole, *J. Vac. Sci. Technol., A*, 2005, **23**, 722–724.

40 A. Peremans, F. Maseri, J. Darville and J.-M. Gilles, *J. Vac. Sci. Technol., A*, 1990, **8**, 3224–3228.

41 P.-T. Howe and H.-L. Dai, *J. Chem. Phys.*, 1998, **108**, 7775–7782.

42 T. L. Gilton, C. P. Dehnbostel and J. P. Cowin, *J. Chem. Phys.*, 1989, **91**, 1937–1938.

43 S. K. Jo and J. M. White, *J. Chem. Phys.*, 1991, **94**, 5761–5764.

44 *CRC Handbook of Chemistry and Physics*, ed. D. R. Lide, Taylor and Francis, 94th edn, 2013–2014.

45 P. Ayotte, J. Gamache, A. D. Bass, I. Fabrikant and L. Sanche, *J. Chem. Phys.*, 1997, **106**, 749–760.

46 M. Michaud and L. Sanche, *J. Electron Spectrosc. Relat. Phenom.*, 1990, **51**, 237–248.

47 V. A. Ukraintsev, T. J. Long, T. Gowl and I. Harrison, *J. Chem. Phys.*, 1992, **96**, 9114–9123.

48 V. A. Ukraintsev, T. J. Long and I. Harrison, *J. Chem. Phys.*, 1992, **96**, 3957–3965.

49 H. Keller-Rudek, G. K. Moortgat, R. Sander and R. Sörensen, *Earth Syst. Sci. Data*, 2013, **5**, 365–373.

50 D. Lackey, J. Schott, B. Straehler and J. K. Sasss, *J. Chem. Phys.*, 1989, **91**, 1365–1376.

51 H. Petek, *J. Chem. Phys.*, 2012, **137**, 091704.

52 E. T. Jensen, *J. Chem. Phys.*, 2008, **128**, 044301.

53 Y. Lilach and M. Asscher, *J. Chem. Phys.*, 2003, **119**, 407–412.

54 R. D. Burbank, *J. Am. Chem. Soc.*, 1953, **75**, 1211–1214.

55 T. Kawaguchi, M. Hijikigawa, Y. Hayafuji, M. Ikeda, R. Fukushima and Y. Tomiie, *Bull. Chem. Soc. Jpn.*, 1973, **46**, 53–56.

56 S. Jørgensen, F. Dubnikova, R. Kosloff, Y. Zeiri, Y. Lilach and M. Asscher, *J. Phys. Chem. B*, 2004, **108**, 14056–14061.

57 S. J. Dixon-Warren, D. V. Heyd, E. T. Jensen and J. C. Polanyi, *J. Chem. Phys.*, 1993, **98**, 5954–5960.

58 X.-L. Zhou, F. Solymosi, P. M. Blass, K. C. Cannon and J. M. White, *Surf. Sci.*, 1989, **219**, 294–316.

59 A. Yamakata, T. Ishibashi and H. Onishi, *J. Phys. Chem. B*, 2002, **106**, 9122–9125.

60 T. Rander, A. Lindblad, I. Bradeanu, G. Öhrwall, S. Svensson and O. Björneholm, *J. Chem. Phys.*, 2014, **141**, 224305.

This journal is © the Owner Societies 2015

Phys. Chem. Chem. Phys., 2015, **17**, 9173–9185 | 9185